ACS OMEGA

Open Access

http://pubs.acs.org/journal/acsodf

Article

[^{45}Ti]Ti-HOPOs: Potential Complexes for the Development of ^{45}Ti PET Imaging Agents

Shefali Saini, N.V.S. Dinesh K. Bhupathiraju, Samith B. Jayawardana, Michael D. Phipps, Jason S. Lewis, Lynn C. Francesconi, Gayan B. Wijeratne, Melissa A. Deri, and Suzanne E. Lapi*

Cite This: *ACS Omega* 2025, 10, 7306−7316

Read Online

ACCESS | Metrics & More | Article Recommendations | Supporting Information

ABSTRACT: Titanium-45 (^{45}Ti) is a radionuclide with desirable physical characteristics for use in positron emission tomography (PET) imaging including a moderate half-life (3.08 h), decay by positron emission (85%), and low mean positron energy of 0.439 MeV. Despite these promising characteristics, the radiochemistry for ^{45}Ti including the development of suitable bifunctional chelators is relatively unexplored compared to that of other radiometals. This work investigated three hydroxypyridinone compounds, viz., 3,2,3-(LI-1,2-HOPO) or C8-HOPO, 3,3,3-(LI-1,2-HOPO) or C9-HOPO, 3,4,3-(LI-1,2-HOPO) or C10-HOPO as potential chelators for ^{45}Ti. Radiolabeling optimization, stability, and biodistribution results demonstrated C9-HOPO to be a promising chelator for ^{45}Ti. In vivo evaluation of the [^{45}Ti]Ti-C9-HOPO complex indicated rapid clearance with no signs of decomplexation.

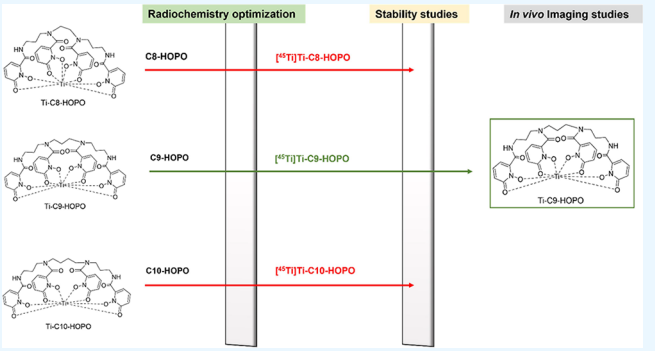

1. INTRODUCTION

The selection of radionuclides and the choice of suitable chelators are important steps in the development of metal-based radiopharmaceuticals. A significant shift has been observed in the field of nuclear imaging in the last few decades with the wider availability of new radiometals and tailored chelators. Several metal-based radiopharmaceuticals have been approved by the United States Food and Drug Administration (FDA) incorporating radiometals such as ^{68}Ga, ^{64}Cu, ^{111}In, ^{201}Tl, ^{99m}Tc, ^{90}Y, and ^{177}Lu.[1−3] Additionally, even more metal-based radiopharmaceuticals are in development at several stages of clinical trials for diagnosis and treatment, generating further interest in exploring novel radioisotopes with suitable properties for radiopharmaceutical development.

Titanium-45 (^{45}Ti) is a radionuclide with excellent physical properties for positron emission tomography (PET), including a half-life of 184.8 min and a decay producing a moderate energy positron (β^+ = 81% and β^+_{mean} = 439 keV). Recent literature reports on ^{45}Ti focus on production and purification methods,[4−7] and some focused studies on radiochemistry development.[8−12] However, the potential of titanium-45 as an imaging agent has been affected by the challenging chemistry of Ti^{4+}.

With the interest toward exploring novel metals, a simultaneous need for suitable chelators is also developing.[13] The majority of commercially used chelators such as DOTA are not ideal because of ineffective binding due to the oxophilic preference of $^{45}Ti^{4+}$. Ideally, chelators for radiometals require fast radiolabeling under mild conditions and high kinetic inertness toward in vivo demetalation.[14] Several studies have been published investigating chelators for ^{45}Ti, as detailed in Table 1. Previous studies by our group investigated the DFO chelator for ^{45}Ti, which required a high pH for efficient radiolabeling, potentially limiting its application.[4] Recently, our group also investigated [^{45}Ti]Ti-THP (hydroxypyridinone functional moiety) and [^{45}Ti]Ti-TREN-CAM (catechol functional moiety) chelators, and both chelators showed rapid radiolabeling (under 30 min) at physiological pH conditions and high in vitro serum stability. In vivo results for [^{45}Ti]Ti-THP indicated signs of decomplexation, while [^{45}Ti]Ti-TREN-CAM showed promising results.[9] More recently, studies with [^{45}Ti]Ti-THP-PSMA indicated promising radiolabeling and in vitro studies, while a low overall tumor uptake was observed through in vivo studies.[15] Recently, Carbo-Bauge et al. investigated a hexadentate 1,2-hydroxypyridinone ligand for applications in PET imaging with ^{45}Ti. While this complex was radiolabeled under physiological conditions (pH 7, 37 °C), in vivo stability studies indicated a labile complex with signs of decomplexation as observed by uptake in heart, liver, and

Received: December 6, 2024
Revised: January 8, 2025
Accepted: January 17, 2025
Published: January 29, 2025

Table 1. Radiolabeling of Chelators Reported in the Literature

			radiolabeling conditions				
#	chelator	functional group	pH	temperature	specific activity (MBq/nmol)	single step	reference
1.	DFO	Hydroxamate	11	37 °C	0.26	yes	4
2.	THP^{Me}	Deferiprone	7−10	37 °C	1.85	yes	9
3.	TREN-CAM	Catechol	6	37 °C	18.5	yes	9
4.	TFPP	Porphyrin	5.5−7	60 °C	0.9	no	10
5.	Ent	Catechol	7	RT[a]	0.1	yes	17
6.	HOPO-O_6-C4	1,2-hydroxypyridinone	7	37 °C	2.4	yes	16
7.	C8-HOPO	1,2-hydroxypyridinone	6	37 °C	13.4	yes	this work
8.	C9-HOPO	1,2-hydroxypyridinone	6	37 °C	2.7	yes	this work
9.	C10-HOPO	1,2-hydroxypyridinone	6	37 °C	2.8	yes	this work

[a]RT: room temperature.

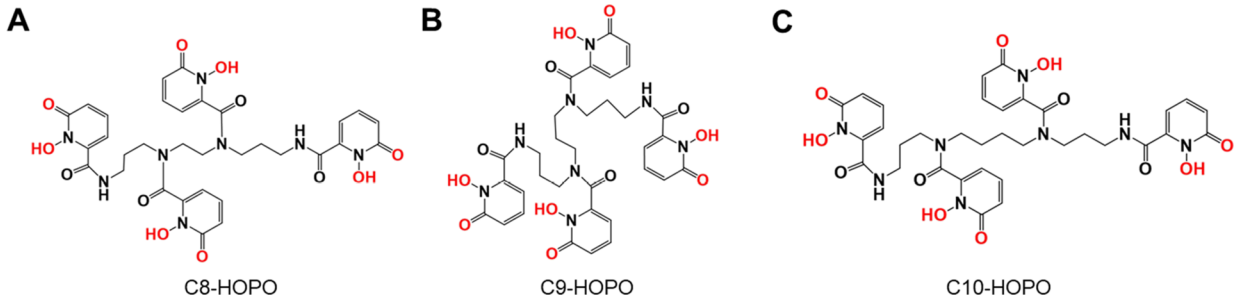

Figure 1. Structures of (A) C8-HOPO (3-2-3-(LI-1,2-HOPO)), (B) C9-HOPO (3-3-3-(LI-1,2-HOPO) and (C) C10-HOPO (3-4-3-(LI-1,2-HOPO).

Scheme 1. Schematic of Synthesis of 1,2-HOPO Ligands

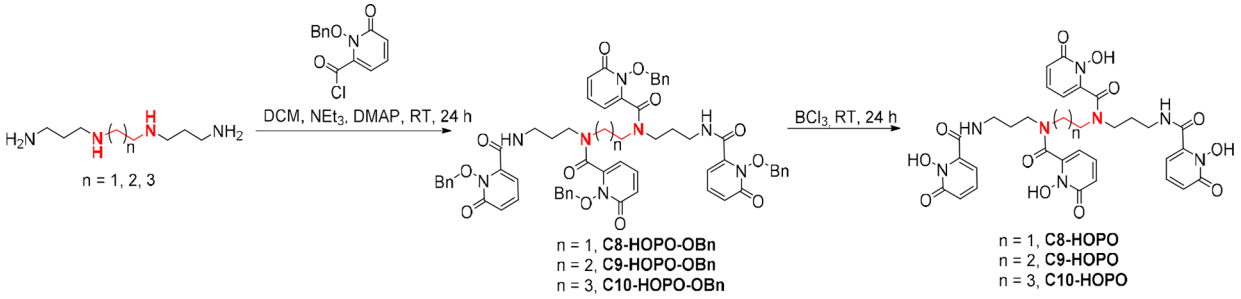

bone.[16] This further indicates a need for structural modification for a stable in vivo formulation. On the other hand, the lack of a stable functionalization site proved a challenge in transitioning the TREN-CAM chelator to the ^{45}Ti radiopharmaceutical stage. A hexacoordinated siderophore enterobactin (Ent) was recently reported by Koller et al. for evaluating catechol-based chelators for ^{45}Ti.[17] Further, a targeting conjugate Ent-DUPA was synthesized, and the radiopharmaceutical potential was evaluated with ^{45}Ti.[17] This was by far the most promising study with ^{45}Ti with significantly higher tumor uptake (8 ± 5%ID/g) in a prostate cancer xenograft model with no signs of decomplexation of radiolabeled complex in vivo. Recently, porphyrin derivatives were labeled with ^{45}Ti by Yekney et al. The complex [^{45}Ti]Ti-TFPP was synthesized by refluxing the solution for 1 h at 60 °C and pH 5.5.[10] Though the complex was formed at high radiolabeling yields (>98%), the reaction time of 1 h, rigorous labeling conditions, and requirement of multistep synthesis might affect the potential of this complex for clinical applications.

1,2-Hydroxypyridinone (HOPO) chelators are known to have a high affinity for hard metal ions in the +3 and +4 oxidation states and form complexes with several radiometals including ^{68}Ga, ^{43}Sc/^{44}Sc/^{47}Sc, ^{89}Zr, ^{177}Lu, and ^{227}Th.[18−20] HOPO complexes have been utilized for multiple applications including MRI contrast agents,[21,22] imaging agents for neurodegenerative disease (Parkinson's and Alzheimer's disease),[23,24] targeted alpha therapy,[25] and photodynamic therapy.[26] The structural features of hydroxamate HOPO compounds allow the formation of a five-membered ring upon metal coordination through the oxygen atoms.[27] Combining the highly basic oxygen donor atoms of four 1,2-HOPO moieties provides an octadentate coordination environment that may result in ligands that would be suitable for the formation of very stable complexes of ^{45}Ti.

The present work investigated the potential of the 1,2-hydroxypyridinone moiety for chelation of [^{45}Ti]Ti^{4+} (Figure 1). Three acyclic ligands (C8-HOPO (3-2-3-(LI-1,2-HOPO)), C9-HOPO (3-3-3-(LI-1,2-HOPO), and C10-HOPO (3-4-3-(LI-1,2-HOPO) were synthesized, characterized, and radiolabeled with ^{45}Ti. These ligands differ by the length of their

https://doi.org/10.1021/acsomega.4c05544
ACS Omega 2025, 10, 7306−7316

linear backbone, and the naming reflects the number of carbon atoms separating the four amine groups in the backbone which each link to one of the 1-2-HOPO units. Macroscopic studies were performed by synthesizing the nonradioactive Ti-HOPO complexes to allow for more complete characterization of the formed Ti-HOPO complexes. In vitro stability in the presence of competing metals and serum proteins was also analyzed, resulting in a lead candidate. In vivo biodistribution studies in naïve mice were performed to understand the kinetic stability of the radiolabeled complexes. Overall, these studies indicated that C9-HOPO holds promise as a ligand for ^{45}Ti.

2. RESULTS AND DISCUSSION

2.1. Synthesis of 1,2-HOPO Ligands. Benzyl protected ligands (C8-HOPO-OBn, C9-HOPO-OBn, and C10-HOPO-OBn) were synthesized using the same synthetic protocol as the published procedure.[18] Then, the targeted ligands (C8-HOPO, C9-HOPO, and C10-HOPO) were synthesized after deprotecting benzyl groups using BCl_3 as the reagent (Scheme 1). All of these compounds were purified using reverse phase HPLC. C10-HOPO was previously synthesized and used as the ligand for different radiometals.[18] All synthesized ligands were flexible and formed rotamers, which resulted in broad multiple peaks in ^{1}H NMR. Multiple peaks were also observed in ^{13}C NMR due to several conformers in each of these ligands. The purity of these ligands was confirmed by HRMS and HPLC. ^{1}H NMR and ^{13}C NMR of C8-HOPO-OBn are available in the Supplementary Figures 1 and 2. ^{1}H NMR and ^{13}C NMR of C9-HOPO-OBn are available in the Supplementary Figures 3 and 4. ^{1}H NMR and ^{13}C NMR of C8-HOPO are available in the Supplementary Figures 5 and 6. ^{1}H NMR and ^{13}C NMR of C9-HOPO are available in the Supplementary Figures 7 and 8.

2.2. Synthesis of Ti-HOPO Complexes. For macroscopic studies, Ti-HOPO complexes were synthesized, and HPLC purified as a single compound. All the synthesized Ti-HOPO complexes were confirmed using analytical HPLC with bare chelators as control (Supplementary Figure 9). The full ^{1}H NMR spectra are shown in Supplementary Figure 10. ^{13}C NMR of Ti-HOPO complex is available in Supplementary Figures 11, 12 and 13 for Ti-C8-HOPO, Ti-C9-HOPO, and Ti-C10-HOPO, respectively. Coelution of the stable Ti-HOPO and radioactive [^{45}Ti]Ti-HOPO complexes on analytical HPLC are shown in Supplementary Figure 14. HRMS confirms each of the Ti-HOPO complexes as shown in Supplementary Figure 15.

Both HPLC and LC-MS chromatograms of all three Ti-HOPO complexes indicated a single species. Analytical HPLC chromatograms for Ti-HOPO complexes are shown in Supplementary Figure 9. The aromatic region of the ^{1}H NMR spectra of the Ti-labeled HOPO complexes is shown in Figure 2. Supplementary Figure 10 shows the full ^{1}H NMR spectra. The aromatic regions of Ti bound HOPO ligands show binding of Ti^{4+} to hydroxypyridinone, and multiple peaks were observed. Two triplets between 7.5 and 8.0 ppm chemical shifts were consistently observed for the protons labeled as H_a. In addition, the aromatic region of Ti-C10-HOPO was indicated by four doublets between 6.2 and 7.2 ppm for protons labeled as H_b (Figure 2A). The NMR pattern was consistent with the previous studies published with Sc-C10-HOPO[28] and Zr-C10-HOPO.[18] Deblonde et al. previously conducted studies with C10-HOPO with hexa and hepta-coordinated species.[29] However, the proposed studies

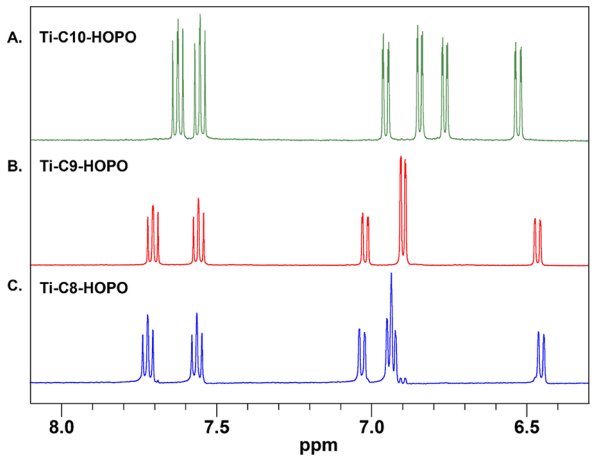

Figure 2. ^{1}H NMR spectra for the aromatic region of (A) Ti-C10-HOPO, (B) Ti-C9-HOPO, and (C) Ti-C8-HOPO.

concluded that the hexacoordinating nature of Ti(IV) using C10-HOPO could result in coordination of 6 out of 8 1,2-HOPO oxygens, while the other 2 oxygen atoms would be available for protonation. As no speciation results were available for comparison, a direct correlation is not possible. For Ti-C9-HOPO (Figure 2B), three doublets were observed between 6.2 and 7.2 ppm. The peak integration for the doublet indicated 2, 4, and 2 protons, indicating a symmetrical structure. The Ti-C8-HOPO structure spectra (Figure 2C) yielded 2 doublets and a triplet indicating overlapping peaks. The number of protons in the aromatic regions summed to 12 for all three ligands. Titanium (Ti^{4+}) complexes are known to have hexa-coordination complexes, while hepta-coordinated and octa-coordinated species are also mentioned in the literature.[30−33] NMR and mass spectra of the synthesized compounds indicated the formation of a single species.

2.3. DFT Calculations. All three complexes are 8-coordinated with respect to the titanium center, and the average Ti−O bond distance exhibits only slight variations (Figure 3). In particular, all Ti−O bond distances are very similar to each other (2.06−2.14 Å), and thus, computation does not predict the ligand backbone to have a large effect on the metal−ligand interactions. In addition to these metal−ligand coordination interactions, a clear intramolecular hydrogen bonding interaction is present between the ligand-based H6 and O2 atoms. We propose that this noncovalent interaction plays a key role in stabilizing the overall complex by restricting the degrees of freedom of the ligand. Intriguingly, the strength of this hydrogen bonding interaction unequivocally increases when going from Ti-C8-HOPO, Ti-C9-HOPO to Ti-C10-HOPO, which may play a crucial role in their stabilities within biological systems (Table 2). So far, these predictions do not match the trends in the stability observed experimentally.

2.4. [^{45}Ti]Ti-HOPO Radiolabeling Optimization. Radiolabeling studies were performed for C8, C9, and C10-HOPO complexes. All three HOPO complexes were radiolabeled with ^{45}Ti rapidly under 30 min incubation at 37 °C. Maximum reaction ratios for >95% radiolabeled complex were 13.4 MBq/nmol (500 μCi/μg), 2.7 MBq/nmol (100 μCi/μg), and 2.8 MBq/nmol (100 μCi/μg) for [^{45}Ti]Ti-C8-HOPO, [^{45}Ti]Ti-C9-HOPO, and [^{45}Ti]Ti-C10-HOPO, respectively. Mass optimization results for the three complexes are represented in Figure 4. HPLC was used to confirm the radiolabeling yield

https://doi.org/10.1021/acsomega.4c05544
ACS Omega 2025, 10, 7306−7316

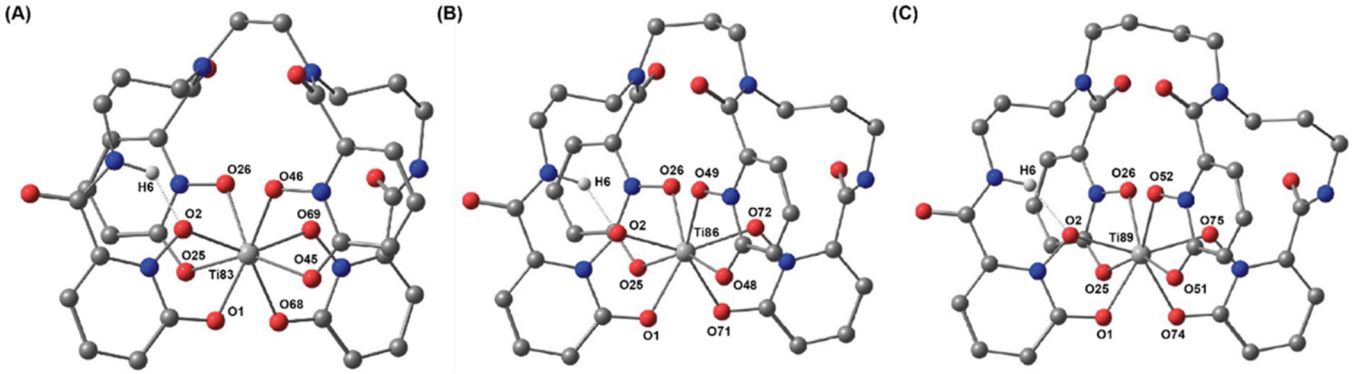

Figure 3. DFT optimized lowest-energy conformers of (A) Ti-C8-HOPO, (B) Ti-C9-HOPO, and (C) Ti-C10-HOPO complexes. Color code: silver = titanium, gray = carbon, red = oxygen, and blue = nitrogen.

Table 2. DFT Optimized Bond Lengths for Ti-C8-HOPO, Ti-C9-HOPO, and Ti-C10-HOPO Complexes at the B3LYP Level of Theory

Ti-C8-HOPO		Ti-C9-HOPO		Ti-C10-HOPO	
Ti83-O2	2.1208 Å	Ti86-O2	2.0929 Å	Ti89-O2	2.1416 Å
Ti83-O69	2.0775 Å	Ti86-O72	2.1050 Å	Ti89-O75	2.0959 Å
Ti83-O26	2.0787 Å	Ti86-O26	2.0863 Å	Ti89-O26	2.1142 Å
Ti83-O46	2.0565 Å	Ti86-O49	2.0825 Å	Ti89-O52	2.0961 Å
Ti83-O1	2.1032 Å	Ti86-O1	2.1429 Å	Ti89-O1	2.1215 Å
Ti83-O68	2.1159 Å	Ti86-O71	2.0954 Å	Ti89-O74	2.1287 Å
Ti83-O25	2.1137 Å	Ti86-O25	2.1256 Å	Ti89-O25	2.0803 Å
Ti83-O45	2.1439 Å	Ti86-O48	2.0948 Å	Ti89-O51	2.0873 Å
H6-O2	1.8229 Å	H6-O2	1.8626 Å	H6-O2	1.8982 Å

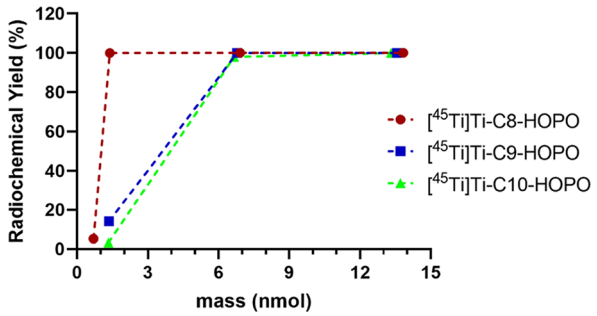

Figure 4. Mass optimization results for [^{45}Ti]Ti-C8-HOPO, [^{45}Ti]Ti-C9-HOPO, and [^{45}Ti]Ti-C10-HOPO. Representative studies were performed at pH 6 and incubation temp of 37 °C for 30 min incubation time.

(Supplementary Figure 11). A single peak for radiolabeled complexes was observed at retention times of 11.20, 11.29, and 11.47 min for [^{45}Ti]Ti-C8-HOPO, [^{45}Ti]Ti-C9-HOPO, and [^{45}Ti]Ti-C10-HOPO, respectively. In addition, iTLC-SG was also used to confirm the radiolabeling where 0.1 M citric acid (pH 5) was used as a mobile phase. Under these conditions, the radiolabeled complex remained at the baseline, while unlabeled [^{45}Ti]Ti-citrate moved with the solvent front.

HPLC coelution studies with [^{45}Ti]Ti-HOPO compounds were performed by injecting with the corresponding stable Ti-C8-HOPO, Ti-C9-HOPO, and Ti-C10-HOPO complexes (Supplementary Figure 11).

2.5. Serum Stability and Metal Challenge Studies. After confirming >95% radiolabeling of HOPO complexes with ^{45}Ti, 100 μL of each radiolabeled complex was mixed with 400 μL of mouse serum and incubated for 6 h. Fractions were collected for analysis at 1, 3, and 6 h time points. [^{45}Ti]Ti-C8-HOPO and [^{45}Ti]Ti-C10-HOPO complexes showed signs of decomplexation, and these complexes were only 55.9 ± 4.9 and 55.5 ± 0.5% intact after 6 h time point (Figure 5A,C).

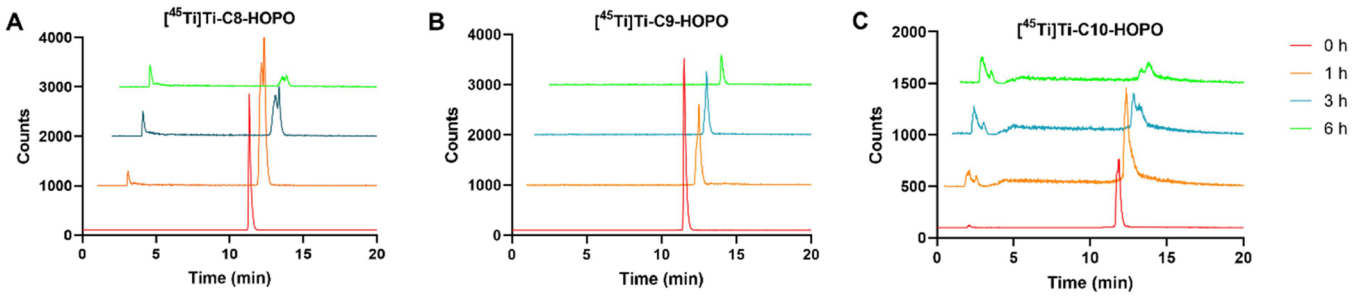

Figure 5. HPLC chromatograms of in vitro stability studies for (A) [^{45}Ti]Ti-C8-HOPO, (B) [^{45}Ti]Ti-C9-HOPO, and (C) [^{45}Ti]Ti-C10-HOPO in mouse serum. HPLC samples were collected at 1, 3, and 6 h postincubation time points (n = 3).

https://doi.org/10.1021/acsomega.4c05544
ACS Omega 2025, 10, 7306−7316

[^{45}Ti]Ti-C9-HOPO was 100% intact with no signs of decomplexation for the entire incubation time of 6 h (Figure 5B). [^{45}Ti]Ti-C8-HOPO and [^{45}Ti]Ti-C10-HOPO complexes degraded as shown by multiple peaks forming as identified by HPLC. Previous studies with C10-HOPO were performed with [^{47}Sc]Sc-HOPO and [^{89}Zr]Zr-HOPO.[28] The results indicated the [^{89}Zr]Zr-C10-HOPO complex to be stable up to 7 d time period in mouse serum as tracked through the longer 78.41 h half-life of ^{89}Zr.[18] Although no direct comparison could be estimated for the stability studies for C8-HOPO and C9-HOPO complexes, DFT structural calculations for Zr-C9-HOPO predicted a tight linkage between the ligand and metal compared to Zr-C10-HOPO (16). This along with the smaller ionic radii for Ti^{4+} can be predicted to contribute toward the better stability of [^{45}Ti]Ti-C9-HOPO complex.

In vitro stability results showed [^{45}Ti]Ti-C9-HOPO as a promising candidate for further studies. [^{45}Ti]Ti-C9-HOPO complexes were 100% intact with EDTA challenge study indicating high stability through 6 h incubation (Supplementary Figure 13). However, metal challenge studies indicate decomplexation in the presence of iron, copper, and zinc metal ions. Metal challenge studies were performed with [^{45}Ti]Ti-C8-HOPO and [^{45}Ti]Ti-C10-HOPO, and the results are reported in Supplementary Figure 13. Both [^{45}Ti]Ti-C8-HOPO and [^{45}Ti]Ti-C10-HOPO decomplexed in the presence of $FeCl_2$ and $CuCl_2$ within 1 h incubation with <10% intact complex. However, the complexes were completely intact in EDTA for the entire incubation. Previous studies with [^{89}Zr]Zr-C10-HOPO confirmed that the complex was stable in the presence of competing metal ions for up to 7 days,[18] while [^{47}Sc]Sc-C10-HOPO complex was not stable for metal ions Cu(II), Fe (II), and Zn(II), and complete decomplexation was observed within the first 30 min of incubation.[28]

2.6. Log $P_{OCT/PBS}$ Measurement. The lipophilicity of radiolabeled HOPO complexes was analyzed by incubating the radiolabeled HOPO chelators with octanol and PBS. Log *P* values for [^{45}Ti]Ti-C8-HOPO, [^{45}Ti]Ti-C9-HOPO, and [^{45}Ti]Ti-C10-HOPO were found to be −1.37, −1.28, and −1.36, respectively, indicating that all complexes are hydrophilic.

2.7. In Vivo Imaging and Ex Vivo Biodistribution Analysis. Based on the results from serum stability studies, [^{45}Ti]Ti-C9-HOPO was found to be suitable for further investigation. Therefore, further in vivo stability was investigated for [^{45}Ti]Ti-C9-HOPO. Mice were imaged immediately after injection for 60 min and at 3 h postinjection. Maximum intensity projections (MIP) were generated and are shown in Figure 6. The first 10 min postinjection frame indicated high blood pool activity and uptake in the liver, kidney, and stomach, which was rapidly cleared from the liver and kidney 1 h postinjection. At 3 h postinjection, the [^{45}Ti]Ti-C9-HOPO complex was mainly cleared with some signal remaining in the large intestine indicating clearance through the hepatobiliary pathway (Figure 6A). PET/CT images indicate a high uptake in gall bladder, which is a common uptake organ for hydroxypyridinone complexes[28,18] Control imaging studies were performed with unchelated Ti ([^{45}Ti]Ti-citrate) to compare the biodistribution and understand the kinetic stability of the tracer. [^{45}Ti]Ti-citrate images showed high background images with visible uptake in vital organs such as the heart, liver, and lung (Figure 6B). Uptake in vital organs was persistent after 3 h injection time point indicating high blood pool activity.

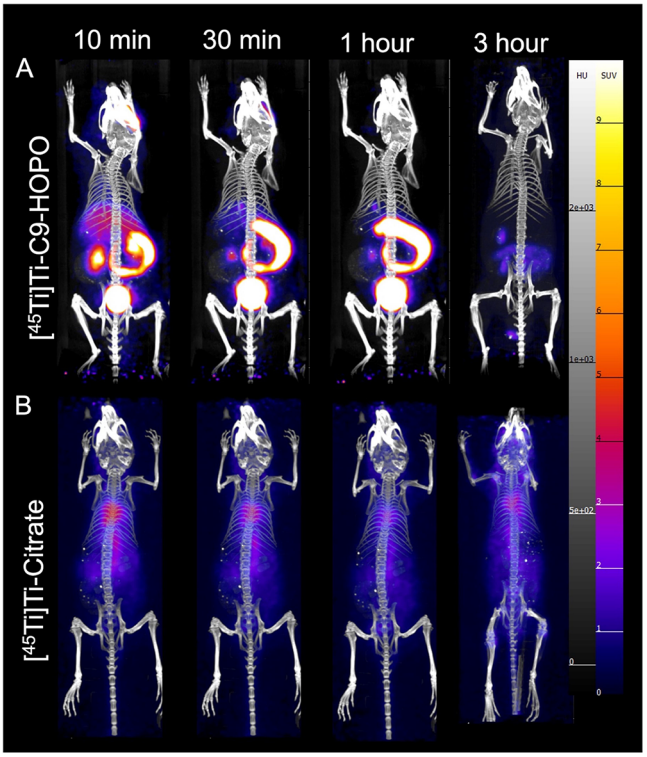

Figure 6. Representative PET/CT images of (A) [^{45}Ti]Ti-C9-HOPO and (B) [^{45}Ti]Ti-citrate. Maximum Intensity Projection slices are compared at 10, 30 min, 1, and 3 h time frames. All images are displayed with SUV scale 0−10.

Regions of interest were generated for the calculation of SUV_{mean} for kidney, heart, lung, muscle, and the combined liver and gall bladder, and time activity curves were generated for these organs with comparison to unchelated Ti ([^{45}Ti]Ti-citrate), as shown in Figure 7. SUV_{mean} data of heart indicated a significantly lower uptake in the heart for [^{45}Ti]Ti-C9-HOPO than [^{45}Ti]Ti-citrate ($p < 0.0001$) (Figure 7A). The SUV_{mean} values indicated a high activity in blood initially, but the compound was rapidly cleared from the heart, as shown in Figure 7A. Conversely, [^{45}Ti]Ti-citrate had persistent uptake in the heart after 3 h time frame as well. Uptake in the liver and gall bladder was high initially in [^{45}Ti]Ti-C9-HOPO, but the uptake was rapidly cleared within 30 min and minimal uptake remained at the 3 h time frame (Figure 7B). Uptake in liver and gall bladder for [^{45}Ti]Ti-citrate was high, and a slow clearance was observed. Uptake in the lungs was significantly lower in [^{45}Ti]Ti-C9-HOPO compared to [^{45}Ti]Ti-citrate ($p < 0.0001$), while persistent uptake in the lungs was observed for [^{45}Ti]Ti-citrate (Figure 7C). Uptake in the kidneys was initially high, but a rapid clearance from the kidneys was observed, as shown in Figure 7D. Low uptake in muscles was observed throughout the 3 h SUV_{mean} time activity frame, while the uptake was significantly lower than [^{45}Ti]Ti-citrate at later time points ($p = 0.0004$) (Figure 7E). Detailed table of time activity curve for heart, liver + gall bladder, lung, kidney and muscle is shown in Supplementary Table 1.

Ex vivo biodistribution data were analyzed to compare the uptake in each organ. [^{45}Ti]Ti-citrate was studied as a control, and the biodistribution patterns were compared to [^{45}Ti]Ti-C9-HOPO. [^{45}Ti]Ti-citrate showed a significant uptake in

https://doi.org/10.1021/acsomega.4c05544
ACS Omega 2025, 10, 7306−7316

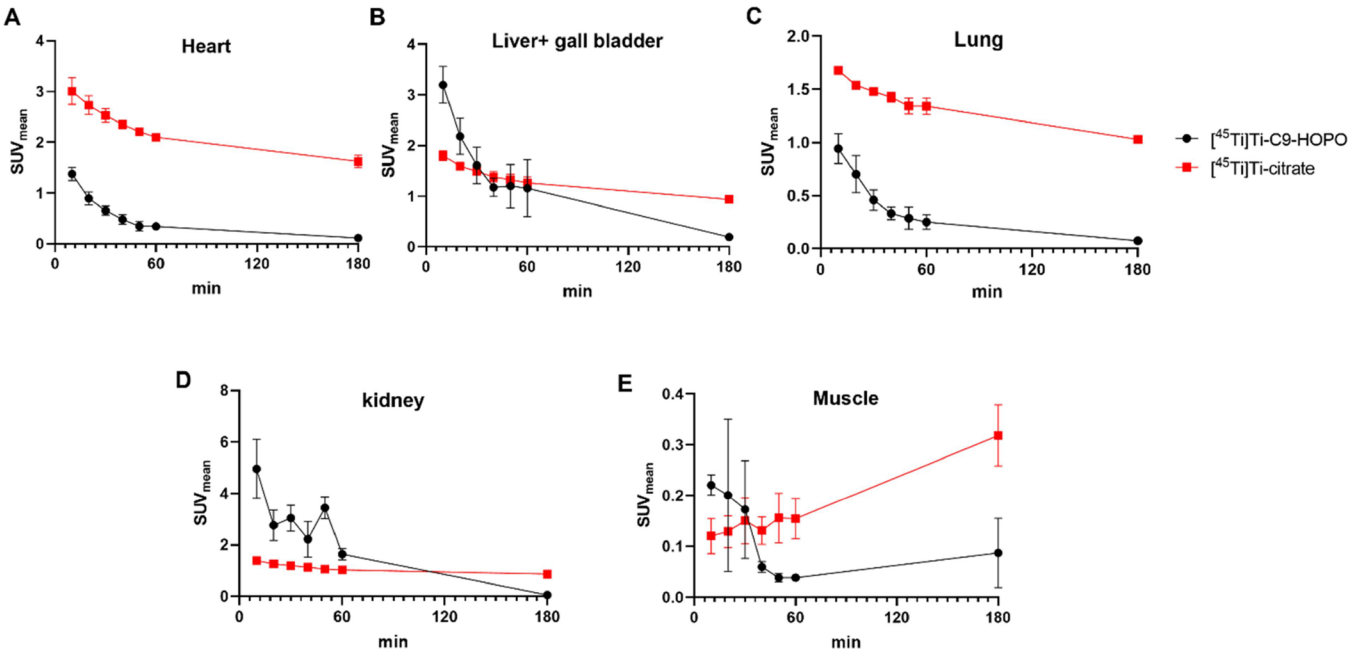

Figure 7. Time activity curves of SUV_{mean} of [^{45}Ti]Ti-C9-HOPO and [^{45}Ti]Ti-citrate for (A) heart, (B) liver and gall bladder, (C) lung, (D) kidney, and (E) muscle for 3 h post-injection imaging time point.

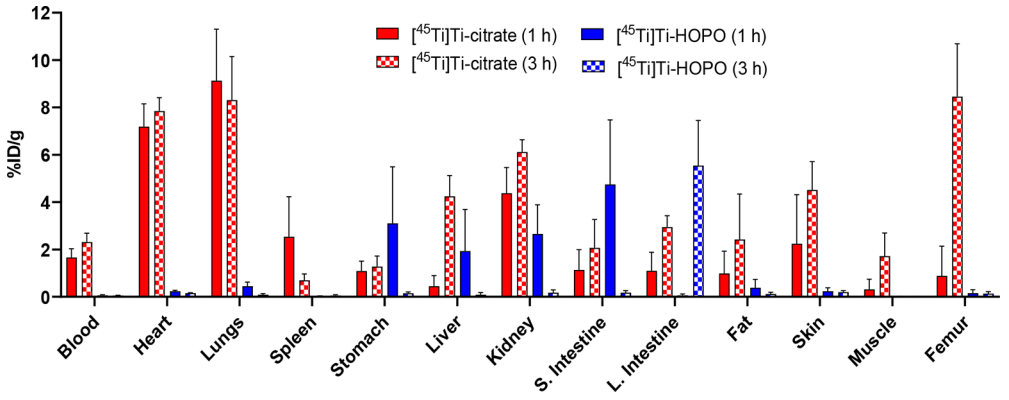

Figure 8. Biodistribution of [^{45}Ti]Ti-C9-HOPO and unchelated [^{45}Ti]Ti-citrate at 1 and 3 h post-injection time point.

blood, heart, liver, and femur, as indicated in Figure 8. Comparing the biodistribution with [^{45}Ti]Ti-C9-HOPO, significantly different biodistribution in blood (2.3 ± 0.4% vs 0.05 ± 0.01%), heart (7.8 ± 0.6% vs 0.16 ± 0.01%), liver (4.2 ± 0.9% vs 0.1 ± 0.1%), and femur (8.5 ± 2.2% vs 0.1 ± 0.1%) was observed for [^{45}Ti]Ti-citrate and [^{45}Ti]Ti-C9-HOPO, respectively. The biodistribution data confirm the kinetic inertness of [^{45}Ti]Ti-C9-HOPO in vivo and no signs of decomplexation. Detailed table of biodistribution for each organ is shown in Supplementary Table 2.

Intending to optimize chelators for the development of ^{45}Ti, we aimed to investigate 1,2-HOPO chelators. The single species [^{45}Ti]Ti-C9-HOPO complex was obtained through mild labeling conditions with high specific activity and in vivo stability. Macroscopic chemistry and tracer studies corresponded well together with a single species formation, as confirmed by HPLC analysis. Mass spectra of nonradioactive Ti-HOPO species further confirmed a 1:1 binding of Ti and 1,2-HOPO derivatives. In vivo imaging study results for Ti-C9-HOPO were promising, with a stable complex with faster clearance through the hepatobiliary excretion route. Though the in vivo studies with [^{45}Ti]Ti-C9-HOPO point toward a stable complex that is rapidly cleared from the body, it would be interesting to see if the complex is stable with a targeting moiety.

Several efforts have been made to improve the solubility and stability of titanium complexes. Heptadentate salan and salen derivatives have been used previously for better solubility and stability. However, even with the improved stability, titanium complexes illustrated low tumor uptake indicating the need to explore more chelator systems.[30] The present study with 1,2-HOPO derivative displayed a high solubility, and C9-HOPO was found to be stable during in vitro and in vivo studies. Future studies require a functionalized version to conjugate HOPO with a targeting vector to further validate the results.

3. MATERIAL AND METHODS

All chemicals were purchased from Sigma-Aldrich unless otherwise stated. Production and separation of Titanium-45 (^{45}Ti) were performed based on previously published methods.[4] ^{45}Ti was eluted as [^{45}Ti]Ti-citrate. Commercially available reagents and solvents (HPLC grade) were purchased

https://doi.org/10.1021/acsomega.4c05544
ACS Omega 2025, 10, 7306−7316

from Sigma-Aldrich and Acros and used without further purification. ^{1}H NMR and ^{13}C NMR spectra were obtained using Bruker Avance III 400 MHz, Bruker Avance DRX 500 MHz, or Bruker Avance III 600 MHz instruments; chemical shifts are expressed in ppm relative to $CDCl_3$ (7.26 ppm, ^{1}H; 77.0 ppm, ^{13}C). Data processing was performed using Bruker topspin 4.1.4 software (Carteret, NJ, USA). NMR spectra were referenced to solvent peaks and expressed on a δ scale. Mass analyses were conducted at the CUNY Mass Spectrometry Facility at Hunter College on an Agilent iFunnel 6550 Q-ToF LC/MS System (for electrospray ionization high-resolution mass spectrometry, HRMS-ESI). The electrospray ionization was run in 95% methanol with 0.1% formic acid. Reactions were monitored by TLC with Analtech Uniplate silica gel G/UV 254 precoated plates (0.2 mm). TLC plates were visualized by iodine vapor. C10-HOPO-OBn was synthesized as per the published procedure, and C10-HOPO was synthesized using BCl_3 instead of HCl.[18] High-performance liquid chromatography (HPLC) purification was performed with 10 × 250 mm (Shimadzu Shim-packed GIST C18 column, H_2O/ACN + 0.1% TFA, 15−25% ACN over 20 min, 10 mL/min) or (Waters Symmetry C18 Column, 100 Å, 5 μm, 4.6 mm × 100 mm, H_2O/ACN + 0.1% TFA, 5−35% ACN over 10 min, 10 mL/min). For macroscopic studies, Agilent 1200 infinity HPLC system was used for analysis and purification. Preparative HPLC purification was performed with SymmetryPrep C18 19 × 100 mm column, while analytical HPLC chromatograms were obtained using a Kromasil Universal C18 4.6 × 250 mm column. UV−Vis spectroscopy was performed on a Thermo Scientific Evolution 220 UV−Visible spectrophotometer. All compounds are >95% pure by HPLC.

All ^{45}Ti samples were analyzed using a CRC-25R dose calibrator from Capintec Inc. (Florham Park, NJ, USA) (calibration # 8445). The dose calibrator was cross-calibrated with Canberra S5000 High-Purity Germanium detector (HPGe). A 1260 Infinity HPLC system (Agilent Technologies, Santa Clara, CA, USA) was used to confirm the radiolabeling yields using a Hypersil gold C18 reverse phase column (Thermo Scientific, Waltham, MA USA). HPLC analysis used a gradient elution with solvent A: H_2O + 0.1% tetrafluoroacetic acid (TFA) and solvent B: acetonitrile (ACN) + 0.1% TFA starting with 100% solvent A (0−5 min) with a gradual increase to 100% solvent B (5−25 min) and switching back to 100% solvent A (25−30 min). T-cell-deficient male mice were purchased from Charles River Laboratory (Wilmington, MA, USA). PET/CT data were acquired on a Sofie GNEXT PET/CT scanner (SOFIE, Dulles, VA, USA). Imaging data were analyzed using Vivo quant (VioQuant 4.0, Invicro Imaging Service and Software, Boston, USA). Data plots were generated with GraphPad Prism software. Ex vivo tissue biodistribution analysis was performed on the HIDEX automatic gamma counter (HIDEX, Turku, Finland).

3.1. Synthesis of 1,2-HOPO Ligands. The synthesis of C10-HOPO (3-4-3-(LI-1,2-HOPO) was previously described.[28] The novel synthesis of C8-HOPO (3-2-3-(LI-1,2-HOPO)) and C9-HOPO (3-3-3-(LI-1,2-HOPO) synthesis is shown in Scheme 1.

3.1.1. 1-(Benzyloxy)-6-oxo-1,6-dihydropyridine-2-carbonyl Chloride. 6.048 g portion (24.69 mmol, 1 equiv) of 1-hydroxy-6-oxo-1,6-dihydropyridine-2-carboxylic acid was suspended in 240 mL of dry dichloromethane under nitrogen. The reaction mixture was placed under ice, and 5.3 mL (7.83 g, 61.72 mmol, 2.5 equiv) of oxalyl chloride was added dropwise, followed by 1 mL catalytic DMF extra dry. Fumes developed. The reaction mixture was left to stir at room temperature for 5 h, a period in which total dissolution of C9-HOPO-OBn was observed, and the solution became dark brown and clear. The reaction mixture was then evaporated to dryness, and the green residue was used directly and immediately in the next reaction without further purification.

3.1.2. Synthesis of 3,2,3-LI(1,2-HOPO)Bn/C8-HOPO-OBn. 0.116 g of N1,N1′-(ethane-1,2-diyl)bis(propane-1,3-diamine) (0.667 mmol, 1 equiv) and 0.01 g (0.073 mmol, 0.10 equiv) of DMAP were added with 0.65 mL (0.473 g, 4.67 mmol, 7 equiv) and 0.65 mL of trimethylamine over ice and stirred for 15 min in 25 mL of dry dichloromethane. 1-(Benzyloxy)-6-oxo-1,6-dihydropyridine-2-carbonyl chloride, 0.87 g (33.366 mmol, 5 equiv), in 25 mL of dry dichloromethane was added dropwise to the mixture containing N1,N1′-(ethane-1,2-diyl)bis(propane-1,3-diamine) over ice, and the reaction mixture was mixed at room temperature for 24 h. The final mixture was evaporated under reduced vacuum and was dissolved in DCM and washed twice with 10% $NaHCO_3$. The organic phase was dried over anhydrous Na_2SO_4, filtered over cotton, and evaporated under reduced vacuum. The crude compound was purified through silica column chromatography using 2−6% of methanol in dichloromethane eluent producing white crystalline foam C8-HOPO-OBn. Yield 60%. ^{1}H NMR (500 MHz, $CDCl_3$): δ 7.63−4.77 (m, 40H), 3.61−1.25 (m, 16H); ^{13}C NMR (125 MHz, CDCl3): δ 162.1, 161.4, 160.8, 160.7, 160.6, 158.5, 158.4, 158.3, 157.9, 143.3, 142.4, 142.2, 139.0, 138.7, 138.6, 138.5, 138.3, 133.5, 133.3, 132.8, 132.6, 131.4, 131.3, 131.2, 131.0, 130.9, 130.8, 130.6, 130.4, 130.3, 130.2, 130.1, 130.0, 129.9, 129.8, 129.7, 129.6, 129.5, 129.4, 128.8, 128.7, 128.6, 128.5, 123.4, 123.3, 123.2, 123.1, 105.1, 105.0, 104.8, 104.7, 104.6, 103.1, 102.2, 80.3, 80.2, 80.1, 45.8, 37.2, 37.0, 36.7.; HRMS calculated for $C_{60}H_{59}N_8O_{12}$ ($[M + H]^+$), 1097.4403, found 1097.4409; calculated for $C_{60}H_{58}N_8O_{12}Na$ ($[M + Na]^+$), 1119.4223, found 1119.4224.

3.1.3. Synthesis of 3,3,3-LI(1,2-HOPO)Bn/C9-HOPO-OBn. 0.125 g of N1,N1′-(propane-1,3-diyl)bis(propane-1,3-diamine) (0.667 mmol, 1 equiv) and 0.01 g (0.073 mmol, 0.10 equiv) of DMAP were added with 0.65 mL (0.473 g, 4.67 mmol, 7 equiv) and 0.65 mL of trimethylamine over ice and stirred for 15 min in 25 mL of dry dichloromethane. 1-(Benzyloxy)-6-oxo-1,6-dihydropyridine-2-carbonyl chloride, 0.87 g (33.366 mmol, 5 equiv), in 25 mL dry dichloromethane was added dropwise to the mixture containing N1,N1′-(propane-1,3-diyl)bis(propane-1,3-diamine) over ice, and the reaction mixture was mixed at room temperature for 24 h. The final mixture was evaporated under a reduced vacuum and was dissolved in DCM and washed twice with 10% $NaHCO_3$. The organic phase was dried over anhydrous Na_2SO_4, filtered over cotton, and evaporated under a reduced vacuum. The crude compound was purified through silica column chromatography using 2−6% of methanol in dichloromethane eluent producing white crystalline form C9-HOPO-OBn. Yield 58%. ^{1}H NMR (500 MHz, CDCl3): δ 7.58−4.99 (m, 40H), 3.19−1.15 (m, 18H). ^{13}C NMR (125 MHz, $CDCl_3$): δ 161.7, 161.3, 161.0, 160.7, 160.6, 158.6, 158.4, 158.2, 157.8, 143.7, 143.6, 143.3, 143.0, 142.7, 142.4, 142.0, 139.0, 138.7, 138.6, 138.3, 138.2, 138.1, 133.6, 133.5, 133.4, 133.3 133.0, 132.8, 132.5, 131.4, 131.1, 131.0, 130.8, 130.7, 130.4, 130.3, 130.2, 129.8, 129.6, 128.8, 128.7, 128.6, 124.0, 123.9, 123.4, 123.2, 123.1, 122.9, 122.8, 121.9, 105.3, 104.7, 104.6, 104.0, 102.4, 102.2, 102.1, 80.5, 80.5, 46.1, 45.7, 43.3, 37.0, 36.9, 26.5. HRMS calculated

https://doi.org/10.1021/acsomega.4c05544
ACS Omega 2025, 10, 7306−7316

for $C_{61}H_{61}N_8O_{12}$ ([M + H]$^+$), 1083.4247, found 1083.4240; calculated for $C_{61}H_{60}N_8O_{12}Na$ ([M + Na]$^+$), 1105.4066, found 1105.4067.

3.1.4. Synthesis of 3,2,3-LI(1,2-HOPO)/C8-HOPO. 0.065 g of C8-HOPO-OBn was dissolved in 70 mL of dry dichloromethane and placed under ice. 1 mL of BCl_3 in p-xylene was added to a vial containing 20 mL of dry dichloromethane. The reaction was run at room temperature for 24 h, during which a light brown precipitate formed. The solid precipitate was filtered over vacuum (0.031 g crude weight), dissolved in water, and purified by preparative HPLC to yield C8-HOPO in 50% yield. ^{1}H NMR (500 MHz, DMSO-d6): δ 7.49−7.61 (m, 4H), 6.84−6.51 (m, 8H), 3.87−3.24 (m, 12H), 2.22−1.71 (m, 4H). ^{13}C NMR (125 MHz, DMSO-d6): δ 163.5, 163.4, 163.3, 163.2, 162.4, 162.0, 161.9, 160.1, 159.9, 159.8, 140.7, 140.5, 140.4, 140.2, 140.1, 139.9, 139.7, 139.6, 139.4, 139.0, 120.9, 120.8, 120.7, 120.4, 120.1, 120.0, 117.5, 108.8, 108.7, 108.3 108.2 106.6, 106.1, 106.0, 47.2, 46.9, 45.7, 45.1, 43.3, 42.6, 27.2, 27.01, 25.6, 25.4. HRMS calculated for $C_{32}H_{35}N_8O_{12}$ ([M + H]$^+$), 723.2369, found 723.2369; calculated for $C_{32}H_{34}N_8O_{12}Na$ ([M + Na]$^+$), 745.2188, found 745.2175.

3.1.5. Synthesis of 3,3,3-LI(1,2-HOPO)/C9-HOPO. 0.065 g portion of C9-HOPO-OBn was dissolved in 70 mL of dry dichloromethane and placed under ice. 1 mL of BCl_3 in p-xylene was added to a vial containing 20 mL of dry dichloromethane. The reaction was run at room temperature for 24 h, during which a light brown precipitate formed. The solid precipitate was filtered over vacuum (0.031 g crude weight,), dissolved in water, and purified by preparative HPLC to yield C9-HOPO in 50% yield. ^{1}H NMR (500 MHz, DMSO-d6): δ 7.50−7.59 (m, 4H), 6.83−6.54 (m, 8H), 3.48−3.26 (m, 12H), 2.03−1.92 (m, 6H). ^{13}C NMR (125 MHz, DMSO-d6): δ 163.0, 162.9, 162.7, 162.4, 162.00, 161.9, 160.1, 160.0, 159.8, 140.8, 140.7, 140.6, 140.5, 140.0, 139.8, 139.7, 139.6, 139.4, 139.0 120.9, 120.8, 120.3, 120.2, 120.0, 119.8, 117.4, 115.1, 108.8, 108.7, 108.2, 108.1, 106.2, 106.0, 105.9, 46.7, 46.6, 46.4, 46.1, 42.7, 42.4, 42.3, 27.1, 25.9 25.8, 25.6, 25.4, 24.1. HRMS calculated for $C_{33}H_{37}N_8O_{12}$ ([M + H]$^+$), 737.2525, found 737.2520; $C_{33}H_{36}N_8O_{12}Na$ ([M + Na]$^+$), 759.2345, found 759.2330.

3.2. Synthesis of Ti-HOPO Complexes. Ti-HOPO complexes were synthesized by mixing an equimolar ratio of titanium(IV) chloride (0.09 M $TiCl_4$ in 20% HCl) and each of the HOPO derivatives (20 mg, C8-HOPO or C9-HOPO or C10-HOPO) in water (10 mL). Upon mixing, a yellow color was observed immediately. This suggested complex formation due to ligand-to-metal charge transfer. Previous literature studies support the formation of yellow coloration with Ti-3,4,3-HOPO complex, as suggested by Deblonde et al.[29] The reaction vial was sonicated in a water bath for 30 min. After 30 min, 2 M K_2CO_3 was used to redissolve the precipitates by increasing the pH of the solution to 8. The reaction vial was sonicated for 30 min followed by a 10 min centrifuge at 4000 g. The supernatant was collected and filtered with a 0.2 μm filter before lyophilization. Lyophilized, Ti-HOPO complexes were dissolved in water and purified by preparative HPLC. Purified fractions were lyophilized and dissolved in D_2O for ^{1}H NMR and ^{13}C NMR. High-resolution mass spectrometry (HRMS) of all three Ti-HOPO compounds was conducted on samples dissolved in water. **Ti-C8-HOPO** ^{13}C NMR (125 MHz, DMSO-d6): δ 162.7, 160.3, 159.8, 158.7, 158.6, 140.1, 139.2, 136.4, 136.0, 113.2, 111.6, 110.2, 43.4, 37.6, 26.7. HRMS was calculated for $C_{32}H_{31}N_8O_{12}Ti$ ([M + H]$^+$), 767.1539, (found 767.1539); calculated for $C_{32}H_{30}N_8O_{12}TiNa$ ([M + Na]$^+$), 789.1358, (found 789.1354). **Ti-C9-HOPO** ^{13}C NMR (125 MHz, DMSO-d6): δ 161.6, 159.8, 159.5, 158.3, 140.2, 138.7, 135.6, 135.4, 112.8, 111.1, 110.5, 109.9, 46.1, 44.3, 36.9, 25.5, 23.3. HRMS was calculated for $C_{33}H_{33}N_8O_{12}Ti$ ([M + H]$^+$), 781.1696, (found 781.1716); calculated for $C_{33}H_{32}N_8O_{12}TiNa$ ([M + Na]$^+$), 803.1515, (found 803.1538). **Ti-C10-HOPO** ^{13}C NMR (125 MHz, D_2O): δ 163.1, 162.9, 162.8, 161.6, 160.0, 159.9, 139.1, 137.9, 137.1, 136.8, 119.8, 117.5, 115.2, 114.4, 112.8, 112.6, 111.9, 110.8, 45.4, 45.2, 36.7, 27.1, 26.5. HRMS was calculated for $C_{34}H_{35}N_8O_{12}Ti$ ([M + H] $^+$), 795.1852, (found 795.1853); calculated for $C_{34}H_{34}N_8O_{12}TiNa$ ([M + Na]$^+$), 817.1672 (found 817.1676).

3.3. DFT Calculations. Density functional theory calculations for Ti(IV)-C8-HOPO, Ti(IV)-C9-HOPO, and Ti(IV)-C10-HOPO complexes were carried out with Gaussian-16 software package[34] at unrestricted B3LYP level of theory,[35] with an LANL2DZ basis set[36] with core potential on titanium and 6-311+G(d,p)[37] on the rest of the atoms (e.g., C, N, O, and H). All of the geometry optimizations and frequency calculations were carried out to verify that none of the local minima contained imaginary frequencies. The bulk solvent effects were modeled using a conductor-like polarizable continuum model (CPCM)[38] with a dielectric constant mimicking H_2O as solvent at temperature = 298.15K.

3.4. [^{45}Ti]Ti-HOPO Radiolabeling Optimization. Radiolabeling optimization studies were conducted for all three [^{45}Ti]Ti-1,2-HOPO complexes. 1 mg/mL stocks for all of the chelators were prepared in water. For initial screening, 18.5 MBq (500 μCi) ^{45}Ti was mixed with varying masses of chelators between 0.6 and 13 nmol (0.5−10 μg) in HEPES buffer (0.1 M, pH 7). The final pH was adjusted to between 5 and 6 for all the radiolabeling studies using NaOH (5 M) keeping the final reaction volume 120 μL. All the reactions were maintained at 37 °C and incubated for 30 min. Radiolabeling yields were confirmed using HPLC and instant thin-layer chromatography (iTLC). No further purification was performed after the radiolabeling yields were confirmed. Coelution studies were performed by injecting [^{45}Ti]Ti-HOPO and a macroscopic Ti-HOPO complex on the HPLC system. All the radiolabeling reactions were repeated 3 times, and the data were plotted on GraphPad Prism.

3.5. Stability and Metal Challenge Studies. The stability of radiolabeled 1,2-HOPO complexes was investigated using mouse serum. 100 μL of radiolabeled complexes were incubated with 400 μL of mouse serum at 37 °C, and samples were collected after 1, 3, and 6 h incubation. For each incubation time point, a 40 μL fraction of incubated complexes was collected in a microcentrifuge tube, and 40 μL of ACN was added to precipitate the serum protein. This mixture was vortexed at 14 × 1000 g for 5 min, and supernatant was collected for HPLC analysis. Each stability study was repeated at least three times, and data plots were generated using GraphPad Prism.

The stability of radiolabeled complexes was further investigated with EDTA and competing metal ions such as $FeCl_2$, $CuCl_2$, and $ZnCl_2$. For the challenge studies, 50 μM radiolabeled complexes were incubated with 5 mM EDTA and 0.5 mM competing metal ions (Fe^{2+}, Cu^{2+}, and Zn^{2+}). Samples were incubated at 37 °C, and fractions were collected for iTLC analysis at 1, 3, and 6 h time points. All analysis was performed in triplicate, and the results were plotted using GraphPad Prism.

https://doi.org/10.1021/acsomega.4c05544
ACS Omega 2025, 10, 7306−7316

3.6. Log P Measurement. Log $P_{OCT/PBS}$ measurements were performed with ^{45}Ti radiolabeled HOPO complexes according to Young et al.[39] Briefly, 450 μL of PBS was mixed with 500 μL of 1-octanol, and this mixture was added to 50 μL fraction of the radiolabeled 1,2-HOPO complexes. After a 30 min incubation, the reaction vial was centrifuged for 10 min at 10,000 rpm to separate the organic (1-octanol) and aqueous phase (PBS). Each phase was collected in a different microcentrifuge vial, and the amount of radioactivity was measured using dose calibrator. The results were reported as logarithms of octanol and PBS concentration.

3.7. In Vivo Imaging and Biodistribution Analysis. PET/CT imaging studies were performed with the [^{45}Ti]Ti-C9-HOPO complex followed by biodistribution analysis. C9-HOPO was radiolabeled with ^{45}Ti at a specific activity of 2.7 MBq/nmol (100 μCi/μg). An injectable dose was prepared by mixing the radiolabeled complex with sterile PBS (1×) with a final injection dose of 2.4 ± 0.2 MBq/100 μL (65 ± 5 μCi/100 μL). Mice were anesthetized under isoflurane and injected retro-orbitally. Immediately after injection, mice were transferred to a small animal PET scanner for a 60 min dynamic PET scan (6 frames; 10 min/frame) followed by a 3 min CT scan. PET data were reconstructed in 6 frames of 10 min each. A second group of mice was imaged 3 h postinjection for 20 min static scan followed by 3 min CT. Images were processed using VivoQuant, and region of interest (ROI) was drawn for heart, kidney, lung, combined liver and gall bladder, and muscle to calculate the mean standard uptake value (SUV_{mean}).

After imaging, 50 μL of blood was drawn by cardiac puncture, while mice were under isoflurane anesthesia. Mice were sacrificed immediately after blood was drawn, and organs of interest were harvested for analysis. Analysis of radiotracer uptake in each organ was performed using a gamma counter, and data were analyzed to calculate the % ID/g. A controlled study with unchelated titanium-45 ([^{45}Ti]Ti-citrate) was also performed to compare the differences in biodistribution results between chelated and unchelated complexes.

4. CONCLUSIONS

We evaluated three 1,2-HOPO ligands to investigate their complexation with titanium-45 (Ti^{4+}). The complexes were synthesized, and macroscopic studies were performed with stable Ti-HOPO complexes. Radiolabeling studies were performed with all three chelators, and rapid radiolabeling was observed at pH 6 and 37 °C incubation under 30 min. High labeling yields of 13.4, 2.7, and 2.8 MBq/nmol were achieved for [^{45}Ti]Ti-C8-HOPO, [^{45}Ti]Ti-C9-HOPO, and [^{45}Ti]Ti-C10-HOPO, respectively. In vitro serum stability assay confirmed [^{45}Ti]Ti-C9-HOPO to be the most stable. Ex vivo biodistribution studies indicated a kinetically stable complexation. The biodistribution of [^{45}Ti]Ti-C9-HOPO was significantly different than that of unlabeled [^{45}Ti]Ti-citrate. Rapid clearance of the chelator was observed in vivo through the hepatobiliary pathway, and no decomplexation was observed 3 h post-injection. This work aims to develop chelators for ^{45}Ti and utilize the characteristic properties of ^{45}Ti for developing a suitable PET imaging isotope. Future work requires a bifunctional conjugation to translate the work toward diagnostic applications.

ASSOCIATED CONTENT

Supporting Information

The Supporting Information is available free of charge at https://pubs.acs.org/doi/10.1021/acsomega.4c05544.

The HPLC chromatograms, mass spectra, ^{1}H NMR, ^{13}C NMR of the HOPO ligands and the Ti-HOPO complexes, metal challenge studies, and table of biodistribution analysis (PDF)

AUTHOR INFORMATION

Corresponding Author

Suzanne E. Lapi − *Department of Radiology and Department of Chemistry, University of Alabama at Birmingham, Birmingham, Alabama 35294, United States*; Email: lapi@uab.edu

Authors

Shefali Saini − *Department of Radiology and Department of Chemistry, University of Alabama at Birmingham, Birmingham, Alabama 35294, United States*; orcid.org/0009-0007-5448-8303

N.V.S. Dinesh K. Bhupathiraju − *Department of Chemistry, City University of New York Hunter College, New York, New York 10021, United States*; orcid.org/0000-0002-5885-3722

Samith B. Jayawardana − *Department of Chemistry and Biochemistry, University of Alabama, Tuscaloosa, Alabama 35487, United States*; orcid.org/0000-0002-6251-7692

Michael D. Phipps − *Department of Chemistry, City University of New York Hunter College, New York, New York 10021, United States; Ph.D. Program in Chemistry, The Graduate Center of the City University of New York, New York, New York 10016, United States; Molecular Pharmacology Program and the Department of Radiology, Memorial Sloan Kettering Cancer Center, New York, New York 10065, United States*

Jason S. Lewis − *Molecular Pharmacology Program and the Department of Radiology, Memorial Sloan Kettering Cancer Center, New York, New York 10065, United States*; orcid.org/0000-0001-7065-4534

Lynn C. Francesconi − *Department of Chemistry, City University of New York Hunter College, New York, New York 10021, United States; Ph.D. Program in Chemistry, The Graduate Center of the City University of New York, New York, New York 10016, United States*; orcid.org/0000-0001-6314-2899

Gayan B. Wijeratne − *Department of Chemistry and Biochemistry, University of Alabama, Tuscaloosa, Alabama 35487, United States*; orcid.org/0000-0001-7609-6406

Melissa A. Deri − *Ph.D. Program in Chemistry, The Graduate Center of the City University of New York, New York, New York 10016, United States; Department of Chemistry, Lehman College of the City University of New York, Bronx, New York 10468, United States*; orcid.org/0000-0003-4186-5572

Complete contact information is available at: https://pubs.acs.org/10.1021/acsomega.4c05544

Notes

The authors declare no competing financial interest.

https://doi.org/10.1021/acsomega.4c05544
ACS Omega 2025, 10, 7306−7316

■ ACKNOWLEDGMENTS

The authors would like to acknowledge the support from the UAB cyclotron facility for all the irradiations. The UAB cyclotron facility is a member of the Department of Energy University Isotope Network and is supported through DESC0021269 (PI: Lapi). This study was conducted and approved by the University of Alabama at Birmingham Institutional Animal Care and Use Committee (IACUC protocol #22649). Imaging studies were supported by the Small Animal Imaging Core through O'Neal Cancer Center P30CA013148. This study was supported in part by the NIH R35 CA232130 which was awarded to JSL and by the NIH P30 CA08748. Authors acknowledge the Alabama supercomputer authority for their service with the DFT calculations. The authors acknowledge Solana Fernandez for her help with injections. The authors acknowledge Christine Schmidt for her assistance in macroscopic studies. This work was supported in part by the Department of Energy Isotope Program's DE-SC0022550, the Horizon-broadening Isotope Production Pipeline Opportunities (HIPPO) program. Ligand synthesis was supported by the National Center for Advancing Translational Sciences of the National Institutes of Health under Award Number UL1TR002384. A patent on the bifunctional p-SCN-Bn-HOPO chelator has been filed with J.S.L., L.C.F., and M.A.D. as inventors.

■ REFERENCES

(1) Perera, M.; Morris, M. J. From Concept to Regulatory Drug Approval: Lessons for Theranostics. *J. Nucl. Med.* **2022**, *63* (12), 1793−1801.
(2) FDA Approved Radiopharamceuticals, 2023.
(3) Johnbeck, C. B.; Knigge, U.; Loft, A.; Berthelsen, A. K.; Mortensen, J.; Oturai, P.; Langer, S. W.; Elema, D. R.; Kjaer, A. Head-to-head comparison of 64Cu-DOTATATE and 68Ga-DOTATOC PET/CT: a prospective study of 59 patients with neuroendocrine tumors. *J. Nucl. Med.* **2017**, *58* (3), 451−457.
(4) Chaple, I. F.; Thiele, K.; Thaggard, G.; Fernandez, S.; Boros, E.; Lapi, S. E. Optimized methods for production and purification of Titanium-45. *Applied Radiation and Isotopes* **2020**, *166*, No. 109398.
(5) Price, R.; Sheil, R.; Scharli, R.; Chan, S.; Gibbons, P.; Jeffery, C.; Morandeau, L. *Titanium-45 as a candidate for PET imaging: production, processing and applications*. In Proceedings of the 15th International Workshop on Targetry and Target Chemsitry Prague, CZ, 2015.
(6) Vāvere, A. L.; Laforest, R.; Welch, M. J. Production, processing and small animal PET imaging of titanium-45. *Nucl. Med. Biol.* **2005**, *32* (2), 117−122.
(7) Koller, A. J.; Wang, L.; Deluca, M.; Glaser, O.; Robis, M. J.; Mixdorf, J. C.; Chernysheva, M. N.; Guzei, I. A.; Aluicio-Sarduy, E.; De Barnhart, T. E. Novo Approaches to the Solid-Phase Separation of Titanium (IV) and Scandium (III): Translating Speciation Data to Selective On-Bead Chelation toward Applications in Nuclear Medicine. *Inorg. Chem.* **2023**, *62* (50), 20655−20665.
(8) Sadeghi, M.; Enferadi, M.; Nadi, H. 45 Ti, a candidate for positron emission tomography: Study of the cyclotron production. *Radiochemistry* **2011**, *53* (4), 411−414.
(9) Koller, A. J.; Saini, S.; Chaple, I. F.; Joaqui-Joaqui, M. A.; Paterson, B. M.; Ma, M. T.; Blower, P. J.; Pierre, V. C.; Robinson, J. R.; Lapi, S. E. A General Design Strategy Enabling the Synthesis of Hydrolysis-Resistant, Water-Stable Titanium (IV) Complexes. *Angew. Chem.* **2022**, *134* (22), No. e202201211.
(10) Yekany, L. V.; Chiniforoush, T. A.; Fazaeli, Y.; Aboudzadeh, M.; Sadeghi, M. Preparation and quality control of a new porphyrin complex labeled with 45Ti for PET imaging. *Appl. Radiat. Isotopes* **2023**, *193*, No. 110650.
(11) Vavere, A. L.; Welch, M. J. Preparation, biodistribution, and small animal PET of 45Ti-transferrin. *J. Nucl. Med.* **2005**, *46* (4), 683−690.
(12) Saini, S.; Lapi, S. E. Titanium-45 (45Ti) Radiochemistry and Applications in Molecular Imaging. *Pharmaceuticals* **2024**, *17* (4), 479.
(13) Price, E. W.; Orvig, C. Matching chelators to radiometals for radiopharmaceuticals. *Chem. Soc. Rev.* **2014**, *43* (1), 260−290.
(14) Cusnir, R.; Imberti, C.; Hider, R. C.; Blower, P. J.; Ma, M. T. Hydroxypyridinone chelators: from iron scavenging to radiopharmaceuticals for PET imaging with gallium-68. *International journal of molecular sciences* **2017**, *18* (1), 116.
(15) Saini, S.; Mullen, G. E.; Blower, P. J.; Lapi, S. E. Radiochemistry and In Vivo Imaging of [45Ti] Ti-THP-PSMA. *Mol. Pharmaceutics* **2024**, *21*, 822−830.
(16) Carbo-Bague, I.; Saini, S.; Cingoranelli, S. J.; Davey, P. R.; Tosato, M.; Lapi, S. E.; Ramogida, C. F. Evaluation of a novel hexadentate 1, 2-hydroxypyridinone-based acyclic chelate, HOPO-O6-C4, for 43Sc/47Sc, 68Ga, and 45Ti radiopharmaceuticals. *Nuclear Medicine and Biology* **2024**, *128-129*, No. 108872.
(17) Koller, A.; Glaser, O.; DeLuca, M.; Motz, R.; Amason, E.; Carbo-Bague, I.; Mixdorf, J.; Guzei, I.; Aluicio-Sarduy, E.; Smilowicz, D. ″Off-Label″ Use of Enterobactin Enables Targeted Imaging of Cancer with Radioactive Ti (IV). *Angew. Chem.* **2024**, *63*, No. e202319578.
(18) Deri, M. A.; Ponnala, S.; Zeglis, B. M.; Pohl, G.; Dannenberg, J.; Lewis, J. S.; Francesconi, L. C. Alternative chelator for 89Zr radiopharmaceuticals: radiolabeling and evaluation of 3, 4, 3-(LI-1, 2-HOPO). *Journal of medicinal chemistry* **2014**, *57* (11), 4849−4860.
(19) Deri, M. A.; Ponnala, S.; Kozlowski, P.; Burton-Pye, B. P.; Cicek, H. T.; Hu, C.; Lewis, J. S.; Francesconi, L. C. p-SCN-Bn-HOPO: a superior bifunctional chelator for 89Zr immunoPET. *Bioconjugate Chem.* **2015**, *26* (12), 2579−2591.
(20) Zhou, X.; Dong, L.; Shen, L. Hydroxypyridinones as a very promising platform for targeted diagnostic and therapeutic radiopharmaceuticals. *Molecules* **2021**, *26* (22), 6997.
(21) Datta, A.; Raymond, K. N. Gd−hydroxypyridinone (HOPO)-based high-relaxivity magnetic resonance imaging (MRI) contrast agents. *Accounts of chemical research* **2009**, *42* (7), 938−947.
(22) Werner, E. J.; Datta, A.; Jocher, C. J.; Raymond, K. N. High-relaxivity MRI contrast agents: where coordination chemistry meets medical imaging. *Angew. Chem., Int. Ed.* **2008**, *47* (45), 8568−8580.
(23) Arduino, D.; Silva, D.; Cardoso, S. M.; Chaves, S.; Oliveira, C. R.; Santos, M. A. New hydroxypyridinone iron-chelators as potential anti-neurodegenerative drugs. *Front. Biosci.-Landmark* **2008**, *13* (17), 6763−6774.
(24) Santos, M. A.; Chaves, S. 3-Hydroxypyridinone derivatives as metal-sequestering agents for therapeutic use. *Future medicinal chemistry* **2015**, *7* (3), 383−410.
(25) Hagemann, U. B.; Wickstroem, K.; Hammer, S.; Bjerke, R. M.; Zitzmann-Kolbe, S.; Ryan, O. B.; Karlsson, J.; Scholz, A.; Hennekes, H.; Mumberg, D. Advances in precision oncology: targeted thorium-227 conjugates as a new modality in targeted alpha therapy. *Cancer Biother. Radiopharm.* **2020**, *35* (7), 497−510.
(26) Curnow, A.; Perry, A.; Wood, M. Improving in vitro photodynamic therapy through the development of a novel iron chelating aminolaevulinic acid prodrug. *Photodiagnosis and photodynamic therapy* **2019**, *25*, 157−165.
(27) Sharma, S.; Baral, M.; Kanungo, B. Recent advances in therapeutical applications of the versatile hydroxypyridinone chelators. *J. Incl. Phenom. Macrocyclic Chem.* **2022**, *102*, 169.
(28) Phipps, M. D.; Cingoranelli, S.; Bhupathiraju, N. D. K.; Younes, A.; Cao, M.; Sanders, V. A.; Neary, M. C.; Devany, M. H.; Cutler, C. S.; Lopez, G. E. Sc-HOPO: A Potential Construct for Use in Radioscandium-Based Radiopharmaceuticals. *Inorg. Chem.* **2023**, *62* (50), 20567−20581.
(29) Deblonde, G. J.-P.; Lohrey, T. D.; Abergel, R. J. Inducing selectivity and chirality in group IV metal coordination with high-

https://doi.org/10.1021/acsomega.4c05544
ACS Omega 2025, 10, 7306−7316

denticity hydroxypyridinones. *Dalton Transactions* **2019**, *48* (23), 8238−8247.
(30) Immel, T. A.; Grützke, M.; Späte, A.-K.; Groth, U.; Öhlschläger, P.; Huhn, T. Synthesis and X-ray structure analysis of a heptacoordinate titanium (IV)-bis-chelate with enhanced in vivo antitumor efficacy. *Chem. Commun.* **2012**, *48* (46), 5790−5792.
(31) Severin, G. W.; Nielsen, C. H.; Jensen, A. I.; Fonslet, J.; Kjær, A.; Zhuravlev, F. Bringing radiotracing to titanium-based antineoplastics: Solid phase radiosynthesis, pet and ex vivo evaluation of antitumor agent [45Ti](salan) Ti (dipic). *Journal of medicinal chemistry* **2015**, *58* (18), 7591−7595.
(32) Melnik, M.; Cozak, D. Titanium Coordination Compounds: Classification and Analysis of Crystallographic and Structural Data. *Rev. Inorg. Chem.* **1986**, *8* (3−4), 221−286.
(33) Baranwal, B.; Jain, A.; Singh, A. Binary Titanium (IV) Metal-organic Frameworks with Multidentate Ligands. *Org. Chem. Curr. Res.* **2011**, *3*, 2161−2401.
(34) Frisch, M.; Trucks, G.; Schlegel, H.; Scuseria, G.; Robb, M.; Cheeseman, J.; Scalmani, G.; Barone, V.; Petersson, G.; Nakatsuji, H. *Gaussian 16 rev. c. 01*, Wallingford, CT, 2016.
(35) Becke, A. D. A new mixing of Hartree−Fock and local density-functional theories. *J. Chem. Phys.* **1993**, *98* (2), 1372−1377.
(36) Wadt, W. R.; Hay, P. J. Ab initio effective core potentials for molecular calculations. Potentials for main group elements Na to Bi. *J. Chem. Phys.* **1985**, *82* (1), 284−298.
(37) Hehre, W. J.; Ditchfield, R.; Pople, J. A. Self—consistent molecular orbital methods. XII. Further extensions of Gaussian—type basis sets for use in molecular orbital studies of organic molecules. *J. Chem. Phys.* **1972**, *56* (5), 2257−2261.
(38) Cossi, M.; Rega, N.; Scalmani, G.; Barone, V. Energies, structures, and electronic properties of molecules in solution with the C-PCM solvation model. *Journal of computational chemistry* **2003**, *24* (6), 669−681.
(39) Young, J. D.; Abbate, V.; Imberti, C.; Meszaros, L. K.; Ma, M. T.; Terry, S. Y.; Hider, R. C.; Mullen, G. E.; Blower, P. J. 68Ga-THP-PSMA: a PET imaging agent for prostate cancer offering rapid, room-temperature, 1-step kit-based radiolabeling. *J. Nucl. Med.* **2017**, *58* (8), 1270−1277.

https://doi.org/10.1021/acsomega.4c05544
ACS Omega 2025, 10, 7306−7316